B1303

# Study on SrO formation and Sr diffusion mechanism in $La_{0.6}Sr_{0.4}Co_yFe_{(1-y)}O_{3-\delta}$ electrode using DFT

**Karthikeyan Saravanabavan (1,2), Cintia Hartmann (2), Gregory Geneste (3), Patrice Tochon (1), Jerome Laurencin (2)**
(1) Genvia SAS, Plaine Saint Pierre 34500 Béziers/France;
(2) Univ. Grenoble Alpes - CEA/LITEN, 17 rue des Martyrs, 38054 Grenoble/France;
(3) CEA, DAM, DIF, F-91297 Arpajon, France / Université Paris-Saclay, CEA, Laboratoire Matière en Conditions Extrêmes, 91680 Bruyères-le-Châtel/France;
Tel.: 04 38 78 21 60, Mobile: +33 7 69 39 23 58
karthikeyan.saravanabavan@cea.fr

## Abstract

In the recent years, Solid Oxide Cell (SOC) has attracted a growing interest due to its many advantages such as high efficiency and good reversibility between fuel cell and electrolysis modes. However, the SOCs durability still needs to be improved for large-scale commercialization. Among the many physical phenomena that contribute to the cell performance degradation, decomposition of the oxygen electrode made of $La_{0.6}Sr_{0.4}Co_{0.2}Fe_{0.8}O_{3-\delta}$ (LSCF) has been identified to be one of the most detrimental (*1*). The LSCF demixing consists in the Sr segregation at the surface, resulting in the formation of strontium based compounds such as SrO that hinder the oxygen exchange between the electrode and the atmosphere (*2*). Despite its crucial importance, the underlying mechanisms controlling the decomposition as well as the impact of the operating conditions are still not well understood. To address these issues, a modeling approach has been adopted combining Density Functional Theory (DFT) (LSCF slab model in fig. a) and thermodynamic computations. Several model reaction mechanisms of SrO formation have been investigated to estimate the rate of LSCF decomposition. In particular, the role of humidity on SrO formation has been elucidated. Moreover, the diffusion mechanism of Sr through A site vacancies and B site vacancies has been investigated using Nudged Elastic Band (NEB) calculations (example in fig. b). Finally, solutions in terms of material composition have been investigated to mitigate Sr segregation.

a)

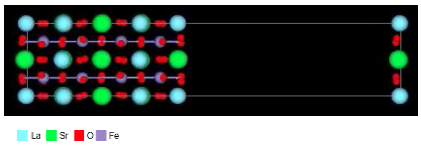


b)

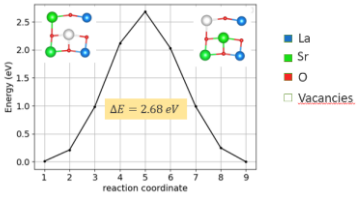


Fig. a) Slab model of LSCF considered for DFT calculations. Fig. b) Energy profile along the diffusion path of Sr element from one A site to its nearest A site vacancy at 0K.

1. F. Monaco *et al.*, *Int. J. Hydrogen Energy*. **46**, 31533–31549 (2021).
2. Z. Pan, Q. Liu, L. Zhang, X. Zhang, S. H. Chan, *J. Electrochem. Soc.* **162**, F1316–F1323 (2015).

## Introduction

Solid oxide cells (SOC) are High Temperature Steam Electrolysers (HTSE) that enable a clean conversion of hydrogen into electricity (fuel cell mode) and vice-versa (electrolysis mode). A SOC is composed of a dense electrolyte in Yittria Stablized Zirconia (YSZ) sandwiched between two porous electrodes. State of the electrodes are: a cermet of Ni and YSZ for hydrogen electrode and a mixed ionic-electronic conductor $La_{0.6}Sr_{0.4}Co_{0.2}Fe_{0.8}O_3$ for the oxygen electrode. This technology is advantageous as it is highly efficient, thanks partly to its high-temperature operating environment and it also does not involve any use of expensive catalysts. Despite these advantages, the technology has not yet been commercialised in the large scale due to high degradation rate upon operation. The loss in performance is attributed mainly to microstructural evolutions and material decomposition of the electrodes. Among the many physical phenomena that contribute to this degradation, decomposition of the LSCF oxygen electrode has been identified to be one of the most detrimental [1-3].

## Litterature review on LSCF decomposition

It is well known that LSCF decomposition by Sr segregation is one of the primary causes of LSCF performance deterioration [4-6]. Sr segregation results particularly in the formation of SrO precipitates, on the electrode surface, which hinders the oxygen exchange kinetics that is crucial to the electrode's electrochemical performance [4]. There is, however, no clear consensus on the impact of operating conditions, such as temperature T and oxygen partial pressure $p_{O_2}$, on Sr segregation and the resulting SrO formation.

On the one hand, it has been shown that performance loss due to Sr segregation is exacerbated with increasing temperatures. Oh *et al.* [7] reported on more pronounced SrO precipitates and increasing areal densities with increasing thermal treatment temperatures ranging between 600°C and 900°C in LSCF pellets. On a similar note, Monaco *et al.* [5] suggested that Sr release is partly promoted by higher temperatures. On the other hand, Ostrovskiy *et al.* [8] has reported that LSCF is relatively stable at very high temperature 1400°C and at temperatures below 600°C, inferring that Sr segregation occurs in a finite interval of temperature. It was argued that insufficient thermal energy limits the Sr segregation at low temperatures and at high temperatures LSCF free surface is more stable. Similarly, Wang *et al.* [6] observed a decrease in Sr segregation at temperatures above 950°C and they have attributed this to the volatilisation of Sr into $Sr(OH)_2$ and the lowering of the equilibrium Sr surface coverages at high temperatures.

Akin to the effect of temperature, there is no clear consensus on the effect of $p_{O_2}$ either. Oh *et al.* [7] reported an increase in Sr segregation with increasing $p_{O_2}$, by comparing LSCF pellets annealed for 50h in 10% and 21% $O_{2(g)}$. Similarly, Lee *et al.* [9] reported higher Sr segregation in LSM films at higher oxygen partial pressures. Contrarily, Ostrovskiy *et al.* [8] have noted that SrO formation peaks out at $p_{O_2}$ = 0.21atm. They speculate that the lack of SrO at high oxygen partial pressures can be attributed to the defect chemistry where high concentrations of lattice oxygen, associated with high oxygen partial pressure environments, stabilizes the Sr in the lattice via coulombic interactions.

In order to understand the fundamental driving forces of Sr segregation and its effects, a modelling approach based on density functional theory can be undertaken and there has been a few publications on this regard [9-11]. Quite recently, Park *et al.* [12], using DFT calculations coupled with thermodynamic calculations, were able to determine the

stability region of LSF as a function of chemical potential of La and Fe, temperature and oxygen partial pressure. They went on to determine energetically favourable surface terminations of LSF slabs, in the region of stability, for a given T and $p_{O_2}$. They showed that at temperature T = 950K, there are two competing surface terminations: SrO termination and Fe-$O_2$ termination with a La rich layer in sub-surface. However, at a higher temperature T=1400°C, Sr-O termination becomes the only energetically favourable surface termination in the stability region, indicating that higher temperatures favour Sr segregation. Furthermore, they noted that Sr segregation with decreasing oxygen chemical potential.

To the best of our knowledge, there are currently no publications, from a DFT modelling perspective, that tackles the SrO formation on LSCF surfaces directly. In particular, the origin of O for SrO still remains at large. Laurencin *et al.* [13] suggested that it could originate from the bulk of the material itself, as more SrO precipitates were observed in electrolysis mode, in which it is well known that the oxygen concentration is higher in the electrode. In this work, DFT simulations coupled with thermodynamic calculations were done to calculate the Gibbs free energy of SrO formation, through two different mechanisms, on LSCF, in dry air conditions, in order to determine firstly the preferred mechanism of SrO formation and secondly to see the effect of temperature $T$ and oxygen partial pressure $p_{O_2}$ on SrO formation.

## 1. Method

To elucidate the origin of O species for the formation of SrO precipitates on LSCF surface, in dry air conditions, the following two model reaction mechanisms are proposed. The model reaction (i) uses oxygen from the LSCF for SrO formation while the model reaction (ii) uses atmospheric oxygen molecule.

(i) $La_{1-x}Sr_xCo_{0.2}Fe_{0.8}O_3 \longrightarrow y\ SrO + La_{1-x}Sr_{x-y}Co_{0.2}Fe_{0.8}O_{3-y}$

(ii) $La_{1-x}Sr_xCo_{0.2}Fe_{0.8}O_3 + y/2\ O_{2(g)} \longrightarrow y\ SrO + La_{1-x}Sr_{x-y}Co_{0.2}Fe_{0.8}O_3$

where the experimental molar concentration of Sr in LSCF is $x_{exp}$=0.4. Reaction enthalpies of the above two reaction mechanisms at $T$ =0K, $\Delta_r H(T = 0K)$ are calculated using DFT (cf. section 1.1 for details). A thermodynamic defect model is constructed to extrapolate the change in Gibbs free energy $\Delta_r G(T, p)$ from $\Delta_r H(T = 0K)$ which enables us to estimate SrO formation in molar concentrations at a given operating condition temperature $T$, and oxygen partial pressure $p_{O_2}$ (cf. section 1.2 for details).

### 1.1 DFT calculations

LSCF has a perovskite structure $ABO_3$ with $La^{3+}$ and $Sr^{2+}$ ions on the A sites, $Co^{3+}$ and $Fe^{3+}$ on B sites. The slab model used for the DFT simulations is shown in fig 1. The model consists of nine alternating layers of type AO and $BO_2$ (fig 1), constituting 2x2x4 pseudo-cubic unit cells [14]. This contains a total of 88 atoms, with 8 Sr atoms at A sites (making the molar concentration of Sr $x_{slab}$=0.4=$x_{exp}$) distributed using special quasi-random structures (SQS) using the Monte-Carlo SQS code implemented in the theoretical automated toolkit [15, 16]. A vacuum layer of 23Å is included in order to create a free surface. A bulk model was then constructed from the slab model by removing the first AO layer on the left and the vacuum space at right. The resulting system contains a total of 80 atoms with 6 Sr atoms, making $x_{bulk}$=0.4=$x_{exp}$. The molar concentration of Co in both these

model is set to be 1.25, which is the closest value to the experimental concentration of 0.2 that can be modelled in a symmetrical system.

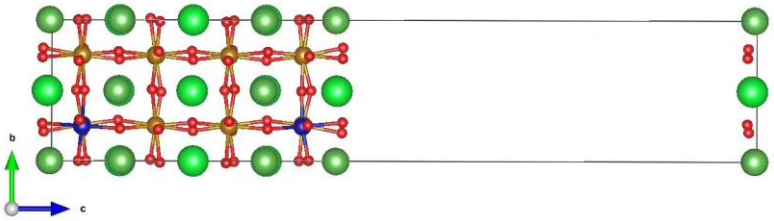


Fig 1: Structure of the LSCF slab model as obtained after structural relaxation

The energetics of SrO formation, via the model reaction mechanisms proposed above, might depend on the exact origin of the Sr atom in LSCF, as the bonding chemistry of Sr is different when it is present on the surface from when it is present in the bulk. The same could be stated about the oxygen atom when it originates from the LSCF for SrO formation. In light of this, seven distinct cases are considered, each differing from one another on the origin of Sr and O species and the model (slab/bulk) used for the calculation, as shown in table 1.

*Table 1 Different cases simulated in DFT calculations on slab model*

| Model | Case # | Origin of O | | Origin of Sr in LSCF |
|---|---|---|---|---|
| LSCF Slab model | 1 | $O_{2(g)}$ | | surf |
| | 2 | | | bulk |
| | 3 | LSCF | bulk | Surf |
| | 4 | | | Bulk |
| | 5 | | surface | Bulk |
| LSCF bulk model | 6 | $O_{2(g)}$ | | Bulk |
| | 7 | Bulk | | |

The calculations were carried out using Kohn-Sham density functional theory and using the ABINIT code [17]. The projected augmented wave method was used with data sets taken from Jollet-Torrent-Holzwarth table (JTH table) [18] and with GGA-PBE0 for the energy functional [19]. In all of the calculations, the plane wave cut-off energy was set to be 20Ha. The self-consistent field (SCF) cycle were terminated when the difference in consecutive maximal forces is less than 1e-6 Ha/Bohr. A 4x4x1 mesh was used for k point sampling of the first Brioullin zone. The Broyden-Fletcher-Goldfarb-Shanno (BFGS) minimization was employed for structural optimization and convergence stopped when all the atomic forces lied below 2e-4 Ha/bohr.

A larger slab, containing 192 atoms was used for cases 1, 3 and 5, as the aforementioned slab didn't manage to converge when there was a vacancy present on the surface of the slab. This is supposed due to the interaction of the surface vacancy with its periodic-self which are close by in the previously described, relatively thin slab. The mesh for k point sampling was set to be 2x2x1 for this slab.

1.2 Thermodynamic defect model

The equilibrium of SrO formation reaction modelled in (i) and (ii) is governed by the change in Gibbs free energy $\Delta_r G(T,p)$. To estimate the quantity of SrO formed via these model reactions, defect models are constructed for all the seven cases. One such case, case 4, will be detailed in this section while the other defect models for other cases are similar in construction.

In case 4, the defect mechanism can be expressed in the following reaction expressed in Kröger-Vink notation (eq: 1):

$$Sr'_{La} + O_O^X = SrO_s + V'''_{La} + V_O^{\blacksquare\blacksquare} \quad \text{(eq. 1)}$$

The above equation corresponds to the reaction where one Sr atom and one O atom from the LSCF is used to form one SrO molecule, creating as a result one A site vacancy and one oxygen vacancy. The change in $\Delta_r G(T,p)$ is zero at equilibrium (eq: 2).

$$\Delta_r G(T,p) = 0 = \Delta_r G°(T,p°) + RTln(K) = \Delta_r H°(T,p°) - T\Delta_r S°(T,p°) + RTln(K) \quad \text{(eq. 2)}$$

where $\Delta_r G°(T,p°)$ is the change in standard Gibbs free energy. $K$ is the equilibrium constant defined as the product of activities $a_i$ of species $i$ involved in the reaction mechanism, raised to the power of its stoichiometric coefficient $\nu_i$ (eq: 3). $\Delta_r H°(T,p°)$ is the change in standard enthalpy and $\Delta_r S°(T,p°)$ the change in standard entropy. $\Delta_r H°(T,p°)$ is approximated to be the change in energy of the reaction at T=0K calculated by the aforementioned DFT calculations [20] (eq: 4). In writing such an expression, we assume SrO as separate entities and not as precipitates which would require the expression of interface energy to be included in $\Delta_r G(T,p)$. $\Delta_r S°(T,p°)$ is assumed negligible in this case [20] (eq: 5).

$$K = \prod_i a_i^{\nu_i} = \frac{[V'''_{La}]\times[V_O^{\blacksquare\blacksquare}]}{[O_O^X]\times[Sr'_{La}]} \quad \text{(eq. 3)}$$

$$\Delta_r H°(T,p°) \approx \Delta_r E_{DFT}(T=0K) = \sum_i \nu_i E_{DFT,i}(T=0K) \quad \text{(eq. 4)}$$

$$\Delta_r S°(T,p°) = S°_{LSCF_{defective}}(T,p°) + S°_{SrO}(T,p°) - S°_{LSCF}(T,p°) \approx 0 \quad \text{(eq. 5)}$$

We assume furthermore that there is no other source of oxygen vacancies in the system and therefore, $[V'''_{La}] = [V_O^{\blacksquare\blacksquare}]$, $[O_O^X] = 3 - [V'''_{La}]$, $[Sr'_{La}] = x - [V'''_{La}]$, equation 2 can be rewritten as $f([V'''_{La}]) = 0$ where $f$ is a second degree polynomial, the resolution of which gives the molar concentration of Sr vacancies and equivalently, molar concentration of SrO formed at a given operating condition temperature $T$.

For cases where the $O_{2(g)}$ is used for the SrO formation, $\nu_{O_2}\mu_{O_{2(g)}}$ is included in the expression of $\Delta_r G(T,p)$. Chemical potential $\mu_{O_{2(g)}}$ of $O_{2(g)}$, in a mixture at temperature $T$ and total pressure of the system $p$, oxygen partial pressure $p_{O_2}$, under ideal gas approximation is defined as follows (eq: 6).

$$\mu_{O_2}(T,p_{O_2},p) = E_{DFT,O_2}(T=0K) + \Delta h°(T°,p°) + Ts°(T°,p°) - Tc_p \ln\left(\frac{T}{T°}\right) + c_p(T-T°) + RTln\left(\frac{p_{O_2}}{p°}\right) \quad \text{(eq: 6)}$$

where $T° = 298.15K$, $p° = 1\ Bar$. $\Delta h°(T°,p°)$ is the change in molar enthalpy at standard pressure and is defined as $\Delta h°(T°,p°) = \Delta h(T=T°,p°) - \Delta h°(T=0K,p°)$. $s°(T°,p°)$ is the molar entropy at standard conditions. $c_p$ is the molar specific heat at constant pressure.

$\Delta h°(T°, p°)$, $s°(T°, p°)$, $c_p$ are taken from JANAF tables [21]. In these cases, the equation $\Delta_r G(T, p) = 0$ is rewritten as $f([V_{La}'''])$ where $f$ is now a third degree polynomial.

## (iii) Results

Reaction enthalpies $\Delta_r H°(T = 0K)$ in eV at T=0K calculated from DFT are reported below in table 2. We notice that in all the listed cases, at T=0K, SrO formation is endothermic in nature. By comparing the values of $\Delta_r H°(T = 0K)$ the preferred origin of O and Sr for SrO formation at 0K can be determined. Upon such comparison we make the following three observations.

Firstly, in comparing case 1 with case 2, where the reaction mechanism differ from one another only by the origin of Sr atom (meanwhile the O is taken from $O_{2(g)}$), we notice that using Sr from the LSCF surface is preferable for SrO formation. We notice an opposite trend in the comparison of case 3 with case 4. This can, however, be explained by the relative positions of Sr and O atoms within LSCF. It must have been easier to create an oxygen vacancy next to a Sr vacancy, which is the situation in case 4, than to create one such vacancy two layers below the Sr vacancy on the surface (case 3).

Secondly, the preferred oxygen species ($O_{2(g)}$ or $O_O^X$) for SrO formation depends on the origin of Sr. When the Sr originates from the surface (case 1 and case 3), the reaction enthalpy for SrO formation is lesser when $O_{2(g)}$ is used $\Delta_r H°(T = 0K)_{case\ 1} < \Delta_r H°(T = 0K)_{case\ 3}$. Whereas when the Sr originates from the bulk of the LSCF (comparison of case 2 with case 4 and case 6 with case 7), the reaction enthalpy is lesser when $O_O^X$ is used for SrO formation.

Lastly, in comparing slab model cases with bulk model cases, i.e.: cases 2 with case 6; cases 4 with case 7; we observe that the presence of a free surface in the slab models lowers the reaction enthalpy $\Delta_r H°(T = 0K)$ slightly.

**Commented [SKG1]:** An intermediate case between these two can be modelled by creating an oxygen vacancy right below the Sr vacancy at sub surface. I expect to find the reaction enthalpy at 0K to be in between the two enthalpies of case 4 and case 3. Something that can be done if we have the time to do so.
I suspect if were to create a slab with both Sr and O vacancy on the surface, the reaction enthalpy would be lower than case 3 and 4.

*Table 2: Results of DFT simulations at T=0K, for different cases simulated*

| Model | Case # | Origin of O | | Origin of Sr in LSCF | $\Delta_r H°(T = 0K)$ in eV |
|---|---|---|---|---|---|
| LSCF Slab model | 1 | $O_{2(g)}$ | | surf | 0.793 |
| | 2 | | | bulk | 1.450 |
| | 3 | LSCF | bulk | Surf | 1.416 |
| | 4 | | | Bulk | 1.284 |
| | 5 | | surface | Bulk | |
| LSCF bulk model | 6 | $O_{2(g)}$ | | Bulk | 1.546 |
| | 7 | Bulk | | | 1.512 |

Molar concentrations of formed SrO, quantified by $[V_{La}''']$, is estimated using the above described model and plotted as a function of temperature T, at oxygen partial pressure $p_{O_2} = 0.21$ Bar and total pressure $p$ = 1 Bar (fig 3). Different coloured curves represent the different cases modelled. The two insets, on the left focuses on case 1 and on the top focuses on cases 2 and 6, as their values are close to zero and are not visible in the main plot. Firstly, we notice that the $[V_{La}''']$ increases with increase in temperature and the overall shape of the curve in all the calculated cases is qualitatively similar. Secondly, it can be noticed that in cases 3,4,7 where the oxygen comes from the LSCF for SrO formation, $[V_{La}''']$ is much higher compared to the rest of the cases in which $O_{2(g)}$ is used for SrO formation. This is also true

for case 7 whose reaction enthalpy at T=0K, $\Delta_r H°(T = 0K)_{case\ 7}$ is higher than that of case 1 and 2.

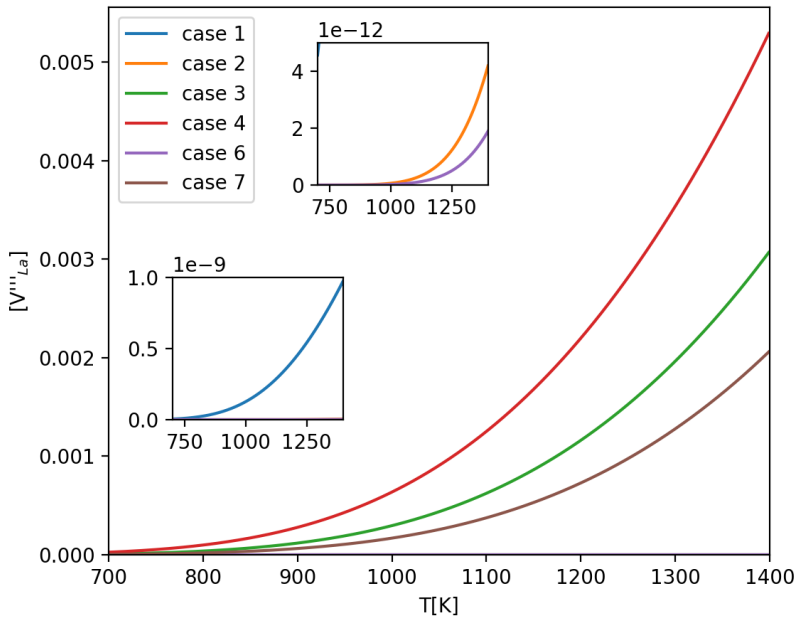


Fig 3: Molar concentration of SrO formed in different modelled cases as a function of temperature T, at oxygen partial pressure $p_{O_2}$=0.21 Bar and total pressure $p$ = 1Bar.

To see the effect of oxygen partial pressure $p_{O_2}$ on cases where O2(g) is used for SrO formation, in fig 4, $[V_{La}'''] $ is plotted as a function of temperature T for case 1, for different oxygen partial pressures $p_{O_2}$ represented as different curves. We notice that with increase oxygen partial pressure, the Sr vacancy concentration increases.

To go further in the analysis of pressure dependency of the SrO formation, we vary the total pressure $p$ of the system from 1 Bar to 30 Bars, while keeping the molar fraction of oxygen constant at 0.21 (fig 5). This is equivalent to taking ambient air and compresses it (increasing both $p$ and $p_{O_2}$ simultaneously). In fig 5, we observe that the Sr vacancy concentration $[V_{La}'''] $ increases with increasing $p$ and increasing $p_{O_2}$.

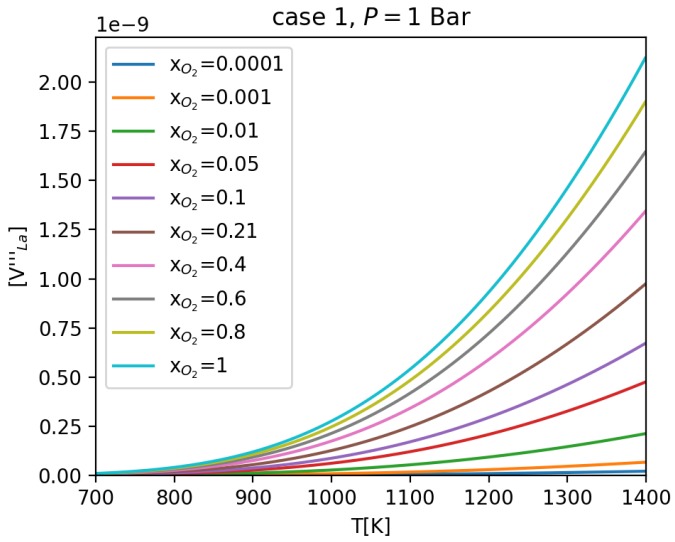


Fig 4: Molar concentration of SrO formed in case 1 as a function of temperature T for different oxygen partial pressures $p_{O_2}$ at total pressure $p$ = 1Bar.

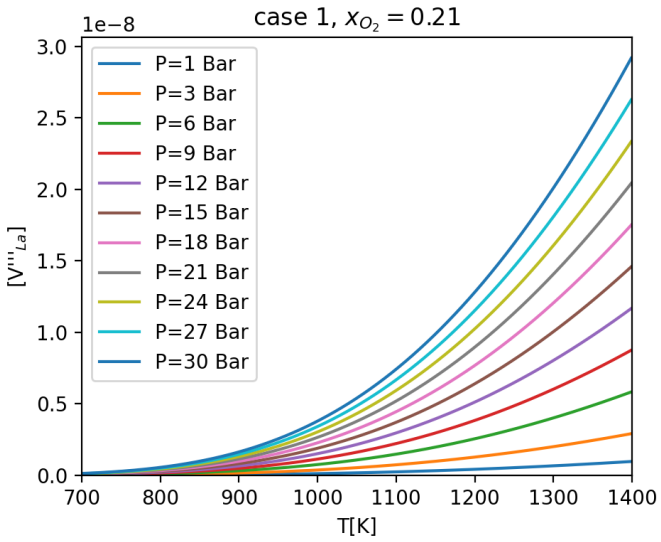


Fig 5: Molar concentration of SrO formed in case 1 as a function of temperature T for different total pressure P and oxygen partial pressures $x_{O2}$=0.21.

## Discussion

In all of the results presented previously, the quantity of Sr vacancy concentration $[V'''_{La}]$ created due to SrO formation, in dry air conditions, remains very small and negligible.

The maximum of Sr vacancy concentration $[V_{La}'''']$, observed in case 4 (fig 3), is in the order of 1e-3 molar concentration which amounts to about only one percent of total Sr present in the system. It can be thus stated that LSCF does not decompose to form SrO, in dry air conditions. This is in good agreement with the recent findings of Sassone *et al.* [22] where they have reported on the absence of LSCF decomposition after operation of 2000 hours at 850°C. They speculate that humidity could be the crucial and perhaps essential for the LSCF decomposition. Supporting this, there are a few publications, which report on the crucial role of water vapour in LSCF decomposition. Zhang *et al.* [23], in their study of LSF oxygen electrodes in presence of water vapour, reported that neither Sr segregation nor its precipitation on the surface are necessary for the decline in electrochemical performance. Instead, they speculate that it is the hydroxylation of the electrode surface that is responsible for the increase in area specific resistance of the electrode. There are DFT studies that support this hydroxylation of the electrode surface that might arise in humid conditions. Geneste *et al.* [24] showed that on $BaTiO_3$, a perovskite structure similar to LSCF, water molecules prefer to be adsorbed through dissociative mechanism, forming two hydroxyl OH-groups, on Ba-O terminations. Similarly, Sharma *et al.* [25] reported a likewise preference of $H_2O$ to be absorbed dissociatively, on bare surfaces (no oxygen vacancies) of LSM slabs. This preferred adsorption mechanism of $H_2O$ can lead to the hydroxylation of the electrode surface. In addition, Kim *et al.* [4] reported large amounts of SrO formation on LSCF electrode under 20 percent humidity while very little was observed in pure $O_2$ flow.

The data shown in fig 5 should be understood with caution. The pseudo-cubic crystal structure taken for LSCF models in the calculations are experimentally relevant only at ambient pressure conditions [14]. Furthermore, we have used the ideal gas approximation for the expression of oxygen chemical potential, which might not be valid at very high pressures. The extrapolations done in fig 5 and the conclusions derived from this figure aim at providing only an heuristic understanding and should not be taken as a comprehensive study of SrO formation at high-pressure environments and very low oxygen partial pressure environments.

The above brings us to the limitations of the methods undertaken in this paper. We have considered the formation of SrO via $O_{2(g)}$ and $O_O^X$. Importantly, the role of water vapour and hydroxylation has been neglected in this work. Furthermore, formation of other Sr based compounds such as $SrCO_3$, $SrZrO_3$, $SrSO_4$ etc… that are also indicative of Sr segregation are excluded in this work. The presence of these Sr based compounds, formed at specific conditions, could facilitate SrO formation at operating conditions. To add on to the list, the kinetic aspect of Sr migration from its perovskite structure to the surface has not been covered in this paper, which may further limit the SrO formation mechanism.

## Conclusion

In this work, two reaction mechanisms for the SrO formation have been proposed: one using the oxygen gas $O_{2(g)}$ from the atmosphere and the other using the oxygen from the LSCF material $O_O^X$. Gibbs free energy of these reactions, in dry air conditions, have been calculated, using DFT calculations coupled with thermodynamic calculations, as a function of temperature T, oxygen partial pressure $p_{O_2}$ and total pressure $p$. We showed that SrO does not form on LSCF, in dry air conditions, in the proposed reaction mechanisms, irrespective of the operating condition (T, $p$, $p_{O_2}$).

## References

1. H. Wang *et al.*, *J. Electrochem. Soc.* **163**, F581–F585 (2016).
2. Z. Pan, Q. Liu, L. Zhang, X. Zhang, S. H. Chan, *J. Electrochem. Soc.* **162**, F1316–F1323 (2015).
3. S. Uhlenbruck, T. Moskalewicz, N. Jordan, H. J. Penkalla, H. P. Buchkremer, *Solid State Ionics*. **180**, 418–423 (2009).
4. D. Kim, J. W. Park, B. H. Yun, J. H. Park, K. T. Lee, *ACS Appl. Mater. Interfaces*. **11**, 31786–31792 (2019).
5. F. Monaco *et al.*, *Int. J. Hydrogen Energy*. **46**, 31533–31549 (2021).
6. H. Wang, S. A. Barnett, *J. Electrochem. Soc.* **165**, F564–F570 (2018).
7. D. Oh, D. Gostovic, E. D. Wachsman, *J. Mater. Res.* **27**, 1992–1999 (2012).
8. E. Ostrovskiy, Y. L. Huang, E. D. Wachsman, *J. Mater. Chem. A*. **9**, 1593–1602 (2021).
9. W. Lee, J. W. Han, Y. Chen, Z. Cai, B. Yildiz, *J. Am. Chem. Soc.* **135**, 7909–7925 (2013).
10. H. Ding, A. V. Virkar, M. Liu, F. Liu, *Phys. Chem. Chem. Phys.* **15**, 489–496 (2013).
11. H. Kwon, W. Lee, J. W. Han, *RSC Adv.* **6**, 69782–69789 (2016).
12. J. Park, J. D. Nicholas, Y. Qi, *Surf. Sci.* **732**, 122268 (2023).
13. J. Laurencin *et al.*, *Electrochim. Acta*. **241**, 459–476 (2017).
14. J. N. Kuhn, U. S. Ozkan, *Catal. Letters*. **121**, 179–188 (2008).
15. S. H. Wei, L. G. Ferreira, J. E. Bernard, A. Zunger, *Phys. Rev. B*. **42**, 9622–9649 (1990).
16. A. Van de Walle, M. Asta, G. Ceder, *Calphad Comput. Coupling Phase Diagrams Thermochem.* **26**, 539–553 (2002).
17. X. Gonze *et al.*, *Comput. Phys. Commun.* **205**, 106–131 (2016).
18. F. Jollet, M. Torrent, N. Holzwarth, *Comput. Phys. Commun.* **185**, 1246–1254 (2014).
19. J. P. Perdew, K. Burke, M. Ernzerhof, *Phys. Rev. Lett.* **77**, 3865–3868 (1996).
20. A. M. Ritzmann, A. B. Muñoz-García, M. Pavone, J. A. Keith, E. A. Carter, *Chem. Mater.* **25**, 3011–3019 (2013).
21. M. W. Chase, Jr., NIST-JANAF Thermochemical Tables. *J. Phys. Chem. Ref. Data Monogr.* **9** (1998), pp. 1–1951.
22. G. Sassone *et al.*, *J. Power Sources*. **605**, 234541 (2024).
23. D. Zhang *et al.*, *Chem. Mater.* **32**, 2926–2934 (2020).
24. G. Geneste, B. Dkhil, , doi:10.1103/PhysRevB.79.235420.
25. V. Sharma *et al.*, *J. Mater. Chem. A*. **4**, 5605–5615 (2016).


*Keywords: LSCF, Sr segregation in dry air conditions, DFT, Defect Model*